## First Indirect Detection Constraints on Axions in the Solar Basin

William DeRocco<sup>®</sup>, <sup>1,\*</sup> Shalma Wegsman, <sup>2,†</sup> Brian Grefenstette<sup>®</sup>, <sup>3,‡</sup> Junwu Huang<sup>®</sup>, <sup>4,§</sup> and Ken Van Tilburg<sup>2,5,||</sup> Santa Cruz Institute for Particle Physics, University of California, Santa Cruz, California 95062, USA <sup>2</sup>Center for Cosmology and Particle Physics, Department of Physics, New York University, New York, New York 10003, USA <sup>5</sup>Cahill Center for Astronomy and Astrophysics, California Institute of Technology, Pasadena, California 91125, USA <sup>4</sup>Perimeter Institute for Theoretical Physics, Waterloo, Ontario N2L 2Y5, Canada <sup>5</sup>Center for Computational Astrophysics, Flatiron Institute, New York, New York 10010, USA

(Received 26 May 2022; revised 1 July 2022; accepted 11 August 2022; published 30 August 2022)

Axions with masses of order keV can be produced in great abundance within the Solar core. The majority of Sun-produced axions escape to infinity, but a small fraction of the flux is produced with speeds below the escape velocity. Over time, this process populates a basin of slow-moving axions trapped on bound orbits. These axions can decay to two photons, yielding an observable signature. We place the first limits on this solar basin of axions using recent quiescent solar observations made by the NuSTAR x-ray telescope. We compare three different methodologies for setting constraints, and obtain world-leading limits for axions with masses between 5 and 30 keV, in some cases improving on stellar cooling bounds by more than an order of magnitude in coupling.

DOI: 10.1103/PhysRevLett.129.101101

Introduction.—The Sun is an exquisite laboratory for new physics. Studies of particles produced in the Sun have provided us with a wealth of information about light, weakly interacting particles, including neutrinos [1–3], axions [4–6], and dark photons [7–9]. Most of these studies have focused solely on the flux of new particles that escape the gravitational potential of the Sun. However, a tiny fraction will be produced at sufficiently small velocities to become gravitationally trapped, forming a "Solar basin" of particles. Reference [10] showed that despite a small injection rate, the local density in this basin can grow appreciably and form a new target for direct detection experiments.

Axions can generically decay, and so a Solar basin may also be indirectly detected through its decay products. In the case of keV-mass axionlike particles [11–15] (hereafter, "axions") with a coupling to photons, axion decays to two photons appear as a narrow line in the x-ray band with a characteristic angular distribution. See Fig. 1 for a schematic depiction of this process. (Aspects of this were foreseen for a Kaluza-Klein axion spectrum in Ref. [16], see also [17].)

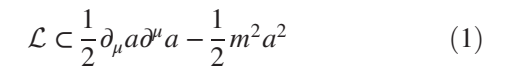
This signal is best probed by x-ray telescopes capable of direct solar observations, such as NuSTAR [18]. While not initially designed as a solar observatory, it has observed both the active Sun [19–21] and the quiescent Sun [22,23],

Published by the American Physical Society under the terms of the Creative Commons Attribution 4.0 International license. Further distribution of this work must maintain attribution to the author(s) and the published article's title, journal citation, and DOI. Funded by SCOAP<sup>3</sup>.

and boasts a subarcminute angular resolution and energy range of 3 to 78 keV.

In this Letter, we analyze a subset of NuSTAR's recent quiescent solar limb dwells to constrain the axion-photon and axion-electron coupling, leveraging the characteristic spatial and spectral features of the basin signal. We place constraints stronger than existing limits [24-27] by about an order of magnitude on the axion-photon and axionelectron couplings for axion masses between 5 and 30 keV. Figures 2 and 3 show our main results, taken along slices of parameter space given by (Fig. 2)  $g_{a\gamma\gamma} = \alpha/2\pi f$  and  $g_{aee} = m_e/f$  where f is the axion decay constant, and (Fig. 3)  $g_{aee} = 0$ . In the following, we employ natural units wherein  $\hbar = c = k_B = 1$ .

Signal.—We consider the leading axion couplings to electrons and photons:



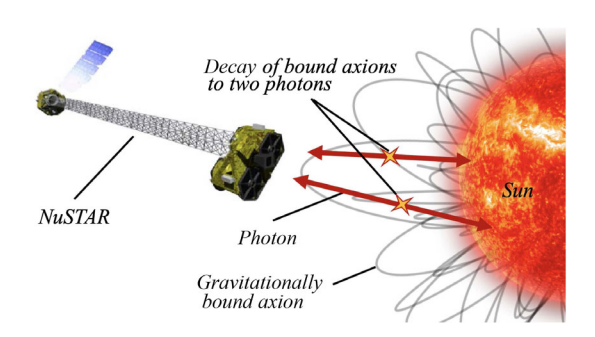


FIG. 1. Solar axions produced on gravitationally bound orbits decay to two (x-ray) photons observable by NuSTAR.

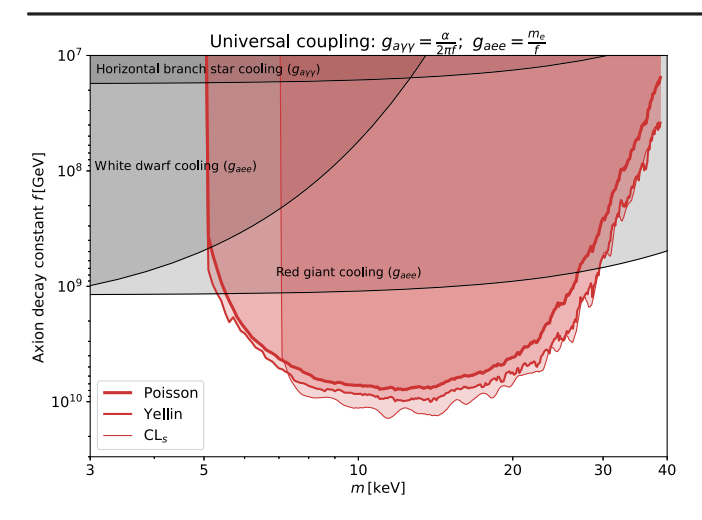


FIG. 2. New limits (90% C.L. on axion parameter space, with couplings determined by the axion decay constant f as  $g_{a\gamma\gamma} = \alpha/2\pi f$  and  $g_{aee} = m_e/f$ . All regions shaded in red are excluded by our analysis. The red curves display the constraints from our three separate analyses: Poisson, optimum cuboid (Yellin) method, and  $CL_s$  limit (see Limits). The gray shaded regions are excluded by stellar cooling [25,28–30].

$$+\frac{g_{aee}}{2m_e}(\partial_{\mu}a)\bar{\psi}_e\gamma^{\mu}\gamma^5\psi_e - \frac{1}{4}g_{a\gamma\gamma}aF_{\mu\nu}\tilde{F}^{\mu\nu}, \qquad (2)$$

where m is the axion mass, a is the axion field,  $g_{aee}$  is the axion coupling to electrons (contributing primarily to axion production), and  $g_{a\gamma\gamma}$  is the axion coupling to photons (allowing decays, and also contributing to production).

The energy density injection rate into the basin at a radius R as a result of these processes has been computed in general in Ref. [10], and can be put into the form

$$\dot{\rho}_{\rm b}(R) \simeq \frac{3}{16\pi} \frac{GM_\odot}{R^4} \int d^3R' \; \tilde{Q}(R') \sqrt{|\Phi(R')|}, \qquad (3)$$

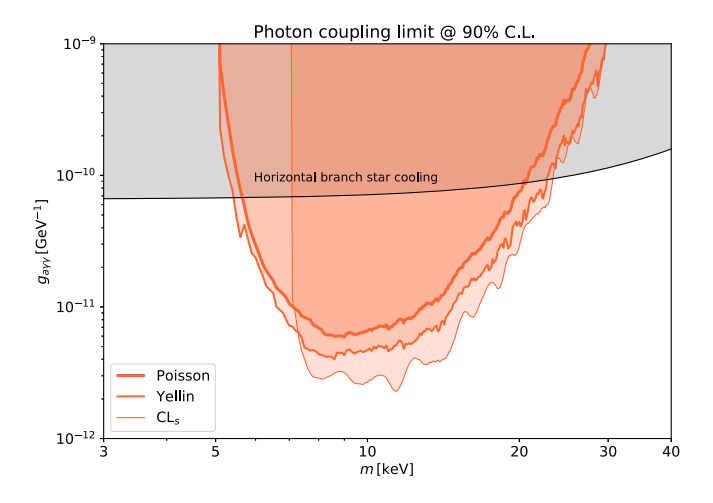


FIG. 3. Limits on the axion-photon coupling  $g_{a\gamma\gamma}$  with  $g_{aee}=0$ . See Fig. 2 for details [30].

where  $M_{\odot}$  is the mass of the Sun and  $\Phi(R')$  is the gravitational potential at the site of production R', with the integral evaluated over the solar volume ( $0 < R < R_{\odot}$ ). The function  $\tilde{Q}(R')$  encapsulates the production rate of nonrelativistic particles into bound orbits [10] and is the sum of three primary components: Compton production  $(\tilde{Q}_C)$ , bremsstrahlung  $(\tilde{Q}_B)$ , and Primakoff production  $(\tilde{Q}_P)$ . Expressions for the first two of these components appear in Ref. [10], and we derive the Primakoff expression

$$\tilde{Q}_{P} = g_{a\gamma\gamma}^{2} \frac{\sqrt{2}\alpha n_{e}T}{\pi^{2} m_{e}} \frac{m^{4}}{m_{e}}$$
(4)

in the Supplemental Material (SM) [31], where  $n_e$  is the electron number density, T the temperature, and  $\alpha$  the fine structure constant. The quantity  $\dot{\rho}_b(R)$  scales quadratically with  $g_{aee}$  (for the  $\tilde{Q}_C$  and  $\tilde{Q}_B$  terms) and  $g_{a\gamma\gamma}$  (for the  $\tilde{Q}_P$  term). We integrate Eq. (3) with all parameters evaluated on the standard solar model of Ref. [42].

The axions in the basin decay to photons ( $a \rightarrow 2\gamma$ ), either directly via their tree-level photon coupling or at loop level via their electron coupling, at the following rate:

$$\Gamma_{\text{rad}} = \frac{g_{a\gamma\gamma}^2 m^3}{64\pi} + \frac{g_{aee}^2 \alpha^2 m^7}{9216\pi^3 m_e^6}$$

$$\approx 2.38 \times 10^{-1} \text{ Gyr}^{-1} \left(\frac{g_{a\gamma\gamma}}{10^{-12} \text{ GeV}^{-1}}\right)^2 \left(\frac{m}{10 \text{ keV}}\right)^3$$

$$+ 5.02 \times 10^{-11} \text{ Gyr}^{-1} \left(\frac{g_{aee}}{10^{-13}}\right)^2 \left(\frac{m}{10 \text{ keV}}\right)^7. \quad (5)$$

If the axion's lifetime  $\Gamma_{\rm rad}^{-1}$  is shorter than the Sun's age  $t_{\odot}=4.6$  Gyr, then the system reaches a steady state in which the rate of basin energy density injection  $(\dot{\rho}_b)$ , which we take to be time-independent) is balanced by the losses due to axion decay  $(\rho_b\Gamma_{\rm rad})$ ; the present-day signal flux is proportional to  $\rho_b\Gamma_{\rm rad}|_{t=t_{\odot}}=\dot{\rho}_b[1-\exp(-\Gamma_{\rm rad}t_{\odot})]$ . We are primarily interested in the region  $R_{\odot} < R < 2R_{\odot}$ , where the majority of basin axions reside, and where secular perturbations from the planets can be neglected [43]. In the SM [31], we argue reabsorption of basin particles can also be ignored for the parameter space considered.

Since axions trapped in the solar basin have low velocities ( $v < v_{\rm esc}$ ), the decay to two photons takes place effectively at rest in the frame of the observer, so each photon acquires an energy  $E_{\gamma} \simeq m/2$ . The spectral signature is therefore a line at x-ray energies.

The angular signature follows from the universal  $1/R^4$  dependence of the basin injection rate [10]. Integrating along a non-Sun-crossing line of sight yields a  $1/\theta^3$  falloff in observed flux with increasing  $\theta$ , where  $\theta$  is the angle from the center of the Sun. Additionally, there is a doubling discontinuity of the signal at the solar limb  $(\theta_{\odot} \equiv \arcsin[R_{\odot}/\mathrm{AU}])$ , where decays obscured by the

Sun for  $\theta < \theta_{\odot}$  become visible when  $\theta > \theta_{\odot}$ . The signal flux can then be put in the more convenient form

$$\begin{split} \frac{dN}{dt dA \mathrm{d}\Omega} &\equiv S_0 T(\theta) = \frac{\dot{\rho}_\mathrm{b}(R_\odot) R_\odot}{6\pi m} [1 - e^{-\Gamma_\mathrm{rad} t_\odot}] T(\theta) \\ &\approx \frac{2.75 \times 10^{-7}}{\mathrm{scm}^2 \, \mathrm{arcsec}^2} \left[ \frac{\dot{\rho}_b(R_\odot) / m}{10^{12} \, \mathrm{cm}^{-3} \, \mathrm{Gyr}^{-1}} \right] [1 - e^{-\Gamma_\mathrm{rad} t_\odot}] T(\theta), \end{split} \tag{6}$$

with  $S_0$  the signal flux per unit solid angle at  $\theta = 0$ . The total number of expected signal events  $\mu$  is the expression of Eq. (6) integrated over the exposure (corrected by live time), ancillary response functions (ARFs), and field of view. An explicit computation of the number flux of signal photons and a plot of the angular template can be found in the SM [31].

Data and analysis.—Data processing: The data used for our analysis were collected by NuSTAR on September 12, 2020, during a series of quiescent limb dwells. Our dataset is taken from the dwell with the least contamination from localized flares (Orbit 2) and further restricted to that orbit's combination of camera head units (CHUs) with maximal live time (CHU12). It is necessary to restrict the data to a particular combination of CHUs in order to ensure the consistency of the spatial coordinates in our analysis. When pointing at the Sun, CHU4 is blinded, hence an uncertainty of 2 arcmin is introduced on the relative pointing direction between different CHU combinations [44]. This pointing error is by far the dominant uncertainty on the signal. Our selection comprises about 1500 s of observations, during which the solar center underwent a 1.26 arcmin shift through NuSTAR's field of view. All events in NuSTAR's calibrated energy range (3-78 keV) were recorded; we plot their spatial distribution in the SM [31].

The photon collection efficiency of NuSTAR over the field of view is quantified in a discrete 13 × 13 partition of subfields for both detectors (A and B), each with angular extent of arcmin × arcmin and separate ARFs computed using the extended-source functionality of the NUPRODUCTS pipeline [44] under the assumption of a spatially uniform background. These ARFs are effective collection areas that take into account detector effects such as aperture stop obscuration, detector absorption, and vignetting [44].

Limits: We set constraints using three methodologies, each with their own benefits and challenges. The first is a Poisson limit, the second is a generalization of the optimum interval method of Refs. [45,46] (to our knowledge, the first multidimensional implementation of the algorithm over binned data), and the third is a likelihood-based  $\mathrm{CL}_s$  method.

*Poisson limit*: The premise behind the Poisson limit is simple: the expected signal counts should not exceed the *total* recorded counts at some level of confidence. We

identify the signal region by integrating over the observation time and spatial coordinates, but restricting to a narrow window in energy  $E \in [m/2 - 2\sigma_E, m/2 + 2\sigma_E]$ , where  $\sigma_E = 0.166$  keV is the spectral resolution (see SM [31]). The 90% confidence limit  $\mu_{\rm lim}$  is set at the value of  $\mu$  (the expected count of signal photons in that interval) such that the cumulative probability for  $\mu > \mu_{\rm lim}$  is less than 0.1. (See SM [31] for details.) This limit-setting procedure suffers from the loss of spatial and temporal information, but sets the standard for the Yellin and  ${\rm CL}_s$  methods discussed below.

Yellin limit: The "Poisson" upper limit discussed above stems from a comparison between the expected signal events and the observed events integrated over the entire field of view and observation time. However, the signal has a known spatial, spectral, and temporal dependence, which can be exploited to mitigate some of the background contamination, even for a completely unknown distribution of the background (Refs. [45,46]). Yellin's method is based on selecting regions within the observed range that contain exceptionally few events in comparison to the signal expectation, or equivalently, exceptionally large regions that contain a given number of events. By construction, this method is relatively insensitive to parts of the signal region with high background (e.g., a flare). The method [45] was designed for searches with a known onedimensional signal distribution, for data that contain few events (e.g., [47]). It is straightforward to find the largest interval that contains a certain number of events, from which one can then find the most improbable of these intervals in the data—the "optimum interval"—by comparing to Monte Carlo simulations with only signal events. Hence, a background-independent limit can be obtained.

In the case of our analysis, the data exist in a four-dimensional space spanned by  $(\alpha, \delta) \equiv (RA, DEC)$  coordinates in the field of view, energy, and time. One important solar background comes from solar (micro)flares, localized features in both space and time. We generalize the optimum interval method to a multidimensional space as outlined in Ref. [46], by identifying the "optimum cuboid" in the four space-energy-time dimensions. This dramatically increases the computational complexity, requiring efficient binning and downsampling strategies (outlined in the SM [31]) that preserve the power of the optimum cuboid method, while handling the high dimensionality and statistics of our data set. As for the Poisson limit, we repeat the procedure for 317 different solar positions, and report the least stringent limit for each value of m.

 ${\rm CL}_s$  method: A (typically) more stringent upper limit can be set with the  ${\rm CL}_s$  method [48], which requires a sufficiently flexible model capable of capturing the background while not overfitting. We make no attempt at modeling the intermittent background from solar (micro) flares. The dominant nonsolar background in most of the energy range of interest arises from cosmic x rays that enter

the detector at a glancing angle, never having passed through the optical bench. Subleading contributions arise from solar lines and internal components of the telescope. We choose to model these three backgrounds using the spectral shapes measured in Ref. [49], but allow their respective normalizations to float; a plot of the spectra is shown in the SM [31]. We treat these backgrounds as spatially uniform, unaffected by the ARFs, since they are not focused by the x-ray optics. Additionally, we raise the minimum energy cutoff for the data to 4 keV to avoid contamination from solar activity. See SM [31] for more detail on the background modeling procedure.

The likelihood can be expressed as a product of Poisson likelihoods over spectral and spatial bins. We add a Gaussian prior around the fiducial solar position with standard deviation  $\sigma_0 = 2$  arcmin. (See SM [31] for the full expression.) For each axion mass m, the model parameters are the signal flux  $S_0$ , the initial solar position, and the normalizations of the three background components. We perform Markov Chain Monte Carlo analyses at each m, and then apply the  $CL_s$  method [48] on the resulting marginalized posterior for  $S_0$  to place constraints.

Results.—The resulting limits are depicted in Figs. 2–4. We represent our results in the three-dimensional parameter space spanned by m,  $g_{a\gamma\gamma}$ , and  $g_{aee}$  in a few different ways. The first is to unify the two couplings in terms of an axion decay constant f via the relations  $g_{a\gamma\gamma} = \alpha/2\pi f$  and  $g_{aee} = m_e/f$ , corresponding to an axion with a tree-level electron coupling, and one-loop anomaly coupling to photons, as in Dine-Fischler-Srednicki-Zhitnisky-type models [50,51]. In this case, the axion is produced mainly through the axion-electron coupling  $(g_{aee})$ , and decays primarily through the axion-photon coupling  $(g_{a\gamma\gamma})$ . This yields the limits displayed in Fig. 2, up to 1 order of magnitude stronger than existing stellar cooling constraints [24–29].

We plot in Fig. 3 the limits in m- $g_{a\gamma\gamma}$  parameter space, with zero axion-electron coupling, where the axion-photon coupling is responsible for both the production and the decay of the axion. These limits also (approximately) apply to the case where the axion-electron coupling is generated at one-loop order, as in Kim-Shifman-Vainshtein-Zakharov-type models [52,53]. Our analysis places a limit on an axion coupling exclusively to photons, over an order of magnitude below existing constraints from horizontal branch star cooling [25].

Finally, we plot our results in  $g_{aee}$ - $g_{a\gamma\gamma}$  space in Fig. 4, with contours corresponding to different axion masses, encapsulating all information at discrete mass values. Tracing a single curve from the upper left to the lower right, one first sees the region in which the axion production is dominated by the Primakoff process, resulting in a bound independent of the electron coupling, and more stringent than horizontal branch star cooling constraints [25] for all but the highest mass displayed. At the dot, the

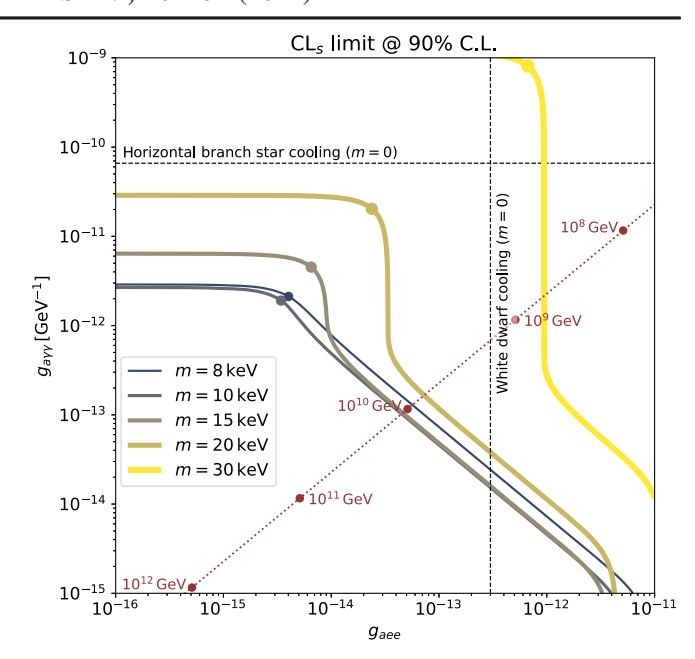


FIG. 4. CL<sub>s</sub> limits on axes of  $g_{a\gamma\gamma}$  and  $g_{aee}$ , with contours denoting different axion masses m. The red dotted line is the slice corresponding to the "universal coupling" displayed in Fig. 2. The dashed lines correspond to stellar cooling constraints (at m=0) [25,28,30].

Compton process overtakes as the dominant production mode, and our constraint becomes independent of  $g_{a\gamma\gamma}$ . At even weaker photon couplings, the axion lifetime starts exceeding the age of the Sun; hence, the basin decay has not yet fully reached detailed balance with the injection rate [see Eqs. (5) and (6)], weakening the constraint to a contour at fixed product  $g_{aee}^2 g_{a\gamma\gamma}^2$ . At very small values of the photon coupling (lower right), the limits become vertical again, indicating the onset of axion decay via an electron loop, occurring well into the region constrained by white dwarf cooling [28] (vertical dashed line). The red dotted line corresponds to the "universal coupling" slice from Fig. 2.

The limits from the optimal cuboid (Yellin) and likelihood ( $\mathrm{CL}_s$ ) methods outperform the Poisson limit over the entire parameter space, as the former two are able to isolate the signal from the background. The optimum cuboid method offers the highest potential gain in datasets with localized, sporadic features such as flares. (In reality, the realized gain is artificially small, as we analyzed a highly quiescent solar period.) Both the Yellin and Poisson limits are completely independent of backgrounds. The likelihood limit typically outperforms the optimum cuboid limit since it includes background fitting of the temporally constant cosmic and instrumental x-ray backgrounds.

Conclusion.—In this Letter, we have presented a first search for x rays from axion decays in the Solar basin, using observations by the NuSTAR telescope. We set new constraints on axion parameter space by over an order of magnitude beyond existing bounds in the mass range of 5 to 30 keV.

Our analysis can be augmented by including a background model of the quiescent, microflaring Sun, which would strengthen the CL<sub>s</sub> limit, and make possible a potential positive detection using the likelihood method. Longer, dedicated solar observations would improve the sensitivity of both the likelihood and optimum cuboid methods. The latter could also tighten with the inclusion of more data, as it automatically selects the least likely region of observation space. Both analyses could also be improved with a more precise knowledge of the fiducial position of the Solar center. A calibration of NuSTAR's ARFs down to lower energies would extend the sensitivity down to about 2 keV.

The Sun is not the only star that can produce an axion basin: compact remnants such as white dwarfs and neutron stars are attractive targets, as are stars with hot, dense cores, such as (super)giants and horizontal-branch stars. Because of its proximity, the Sun produces the largest flux from decays of any axion basin in most of the mass range studied in this work, so solar-limb observations of the quiescent Sun should be the most sensitive probe. For targets with extremely low backgrounds, the smaller signal fluxes from these more distant sources could be compensated by stacking multiple exposures. Such strategies could extend the first-of-its-kind indirect detection search for a stellar basin presented here to a larger mass range (both lower and higher), perhaps even smaller couplings, and other weakly coupled particles, such as dark photons [54] and millicharged particles [55], though they would require knowledge of each target's stellar evolution (age, composition, progenitor), and are thus left to future work. As we have shown in this Letter, indirect detection of stellar basins can probe heretofore unexplored parameter space for weakly coupled particles. With the plethora of extensions outlined above, stellar basins will be an exciting target in the hunt for new physics beyond the standard model.

The data and code are available on GitHub [30].

We thank Iain Hannah, Crystal Kim, and David Smith for discussion regarding NuSTAR data products and instrumental response. We are grateful to Robert Lasenby for sharing preliminary results upon which the production computation in the Supplemental Material [31] is based, as well as many clarifying discussions and comments on the draft. We thank Asimina Arvanitaki and Matthew Johnson for comments on the draft, and Andrea Caputo, Joshua Foster, Cristina Mondino, Benjamin Safdi, Edoardo Vitagliano, and Huacheng Yu for useful conversations. W. D. is supported by the U.S Department of Energy, Grant No. DE-SC0010107. Research at Perimeter Institute is supported in part by the Government of Canada through the Department of Innovation, Science and Economic Development Canada and by the Province of Ontario through the Ministry of

Colleges and Universities. The Center for Computational Astrophysics at the Flatiron Institute is supported by the Simons Foundation.

- \*Corresponding author.
  wderocco@stanford.edu

  †Corresponding author.
  srw9487@nyu.edu

  \*Corresponding author.
  bwgref@srl.caltech.edu

  \*Corresponding author.
- jhuang@perimeterinstitute.ca Corresponding author.
- kenvt@nyu.edu; kvantilburg@flatironinstitute.org
- [1] J. N. Bahcall and R. K. Ulrich, Rev. Mod. Phys. 60, 297 (1988).
- [2] L. Wolfenstein, Phys. Rev. D 17, 2369 (1978).
- [3] S. P. Mikheyev and A. Y. Smirnov, Yad. Fiz. 42, 1441 (1985).
- [4] G. G. Raffelt, Stars as Laboratories for Fundamental Physics: The Astrophysics of Neutrinos, Axions, and Other Weakly Interacting particles (University of Chicago Press, Chicago, 1996), ISBN 978-0-226-70272-8.
- [5] G. Raffelt and L. Stodolsky, Phys. Rev. D 37, 1237 (1988).
- [6] G. G. Raffelt, Lect. Notes Phys. 741, 51 (2008).
- [7] H. An, M. Pospelov, and J. Pradler, Phys. Lett. B 725, 190 (2013).
- [8] J. Redondo and G. Raffelt, J. Cosmol. Astropart. Phys. 08 (2013) 034.
- [9] E. Hardy and R. Lasenby, J. High Energy Phys. 02 (2017) 033.
- [10] K. Van Tilburg, Phys. Rev. D 104, 023019 (2021).
- [11] S. Weinberg, Phys. Rev. Lett. 40, 223 (1978).
- [12] F. Wilczek, Phys. Rev. Lett. 40, 279 (1978).
- [13] R. D. Peccei and H. R. Quinn, Phys. Rev. Lett. 38, 1440 (1977).
- [14] A. Arvanitaki, S. Dimopoulos, S. Dubovsky, N. Kaloper, and J. March-Russell, Phys. Rev. D **81**, 123530 (2010).
- [15] P. Svrcek and E. Witten, J. High Energy Phys. 06 (2006) 051.
- [16] L. DiLella and K. Zioutas, Astropart. Phys. 19, 145 (2003).
- [17] M. Bastero-Gil, C. Beaufort, and D. Santos, J. Cosmol. Astropart. Phys. 10 (2021) 048.
- [18] F. A. Harrison *et al.* (NuSTAR Collaboration), Astrophys. J. **770**, 103 (2013).
- [19] K. Cooper, I. G. Hannah, B. W. Grefenstette, L. Glesener, S. Krucker, H. S. Hudson, S. M. White, D. M. Smith, and J. Duncan, Mon. Not. R. Astron. Soc. 507, 3936 (2021).
- [20] L. Glesener, S. Krucker, I. G. Hannah, H. Hudson, B. W. Grefenstette, S. M. White, D. M. Smith, and A. J. Marsh, Astrophys. J. 845, 122 (2017).
- [21] J. Duncan, L. Glesener, B. W. Grefenstette, J. Vievering, I. G. Hannah, D. M. Smith, S. Krucker, S. M. White, and H. Hudson, Astrophys. J. 908, 29 (2021).
- [22] A. J. Marsh, D. M. Smith, L. Glesener, I. G. Hannah, B. W. Grefenstette, A. Caspi, S. Krucker, H. S. Hudson, K. K. Madsen, S. M. White *et al.*, Astrophys. J. **849**, 131 (2017).

- [23] S. Paterson, I. Hannah, B. Grefenstette, H. Hudson, S. Krucker, and L. Glesener, in AAS/Solar Physics Division Meeting (2020), vol. 52, p. 210.13.
- [24] M. Tanabashi *et al.* (Particle Data Group), Phys. Rev. D 98, 030001 (2018).
- [25] A. Ayala, I. Domínguez, M. Giannotti, A. Mirizzi, and O. Straniero, Phys. Rev. Lett. 113, 191302 (2014).
- [26] F. Capozzi and G. Raffelt, Phys. Rev. D 102, 083007 (2020).
- [27] M. Giannotti, I. G. Irastorza, J. Redondo, A. Ringwald, and K. Saikawa, J. Cosmol. Astropart. Phys. 10 (2017) 010.
- [28] M. M. Bertolami, B. E. Melendez, L. G. Althaus, and J. Isern, J. Cosmol. Astropart. Phys. 10 (2014) 069.
- [29] N. Viaux, M. Catelan, P.B. Stetson, G.G. Raffelt, J. Redondo, A. A. R. Valcarce, and A. Weiss, Phys. Rev. Lett. 111, 231301 (2013).
- [30] The data and code for this Letter are available on GitHub, https://github.com/kenvantilburg/luminous-basin.
- [31] See Supplemental Material, which includes Refs. [32–41], at <a href="http://link.aps.org/supplemental/10.1103/PhysRevLett">http://link.aps.org/supplemental/10.1103/PhysRevLett</a> .129.101101 for further discussions of basin formation, analysis strategy, and resulting limits on parameter space.
- [32] G. G. Raffelt, Phys. Rev. D 33, 897 (1986).
- [33] T. Altherr, Ann. Phys. (N.Y.) 207, 374 (1991).
- [34] T. Altherr and U. Kraemmer, Astropart. Phys. 1, 133 (1992).
- [35] T. Altherr, E. Petitgirard, and T. del Rio Gaztelurrutia, Astropart. Phys. 2, 175 (1994).
- [36] W. DeRocco, M. Galanis, and R. Lasenby, J. Cosmol. Astropart. Phys. 05 (2022) 015.
- [37] K. J. H. Phillips, C. Chifor, and B. R. Dennis, Astrophys. J. 647, 1480 (2006).

- [38] B. W. Grefenstette et al., Astrophys. J. 826, 20 (2016).
- [39] D. Foreman-Mackey, D. W. Hogg, D. Lang, and J. Goodman, Publ. Astron. Soc. Pac. 125, 306 (2013).
- [40] L.-p. Ku, B. Liu, and W. Hsu (1997).
- [41] S. Nandy and B. Bhattacharya, Comput. Math. Appl. 36, 11 (1998).
- [42] N. Vinyoles, A. M. Serenelli, F. L. Villante, S. Basu, J. Bergström, M. Gonzalez-Garcia, M. Maltoni, C. Peña-Garay, and N. Song, Astrophys. J. 835, 202 (2017).
- [43] C. Giovanetti, R. Lasenby, and K. Van Tilburg (to be published).
- [44] M. e. a. Perri, The nustar data analysis software guide, http:// heasarc.gsfc.nasa.gov/docs/nustar/analysis/nustar\_swguide .pdf.
- [45] S. Yellin, Phys. Rev. D 66, 032005 (2002).
- [46] S. Yellin, arXiv:0709.2701.
- [47] S. Henderson, J. Monroe, and P. Fisher, Phys. Rev. D 78, 015020 (2008).
- [48] A. L. Read, J. Phys. G 28, 2693 (2002).
- [49] D. R. Wik et al., Astrophys. J. 792, 48 (2014).
- [50] M. Dine, W. Fischler, and M. Srednicki, Phys. Lett. 104B, 199 (1981).
- [51] A. R. Zhitnitsky, Sov. J. Nucl. Phys. 31, 260 (1980).
- [52] J. E. Kim, Phys. Rev. Lett. 43, 103 (1979).
- [53] M. A. Shifman, A. I. Vainshtein, and V. I. Zakharov, Nucl. Phys. B166, 493 (1980).
- [54] R. Lasenby and K. Van Tilburg, Phys. Rev. D 104, 023020 (2021).
- [55] A. Berlin and K. Schutz, Phys. Rev. D 105, 095012 (2022).